Utilization of four-component scattering power decomposition method for glaciated terrain classification

Gulab Singh, Y. Yamaguchi, and S-E. Park

Graduate School of Science and Technology,
Niigata University, Ikarashi 2-8050, Niigata, 950-2181, Japan

Abstract---Glaciated terrain classification is important for hydrological and climate change modeling. For this purpose, fully polarimetric Advanced Land Observation Satellite-Phase Array L-band Synthetic Aperture Radar (ALOS-PALSAR) data has been used over Indian Himalayan glaciated region. PALSAR data has been analyzed based on **the** three and four component scattering decomposition **methods** for glaciated terrain classification. These **methods** have been applied on multi-looked 3×3 coherency matrix of ALOS-PALSAR data. The analysis of these methods shows that **the Freeman and Durden Three Component Scattering Power Decomposition (3-CSPD) method** has over estimation problem in volume backscattering component as compared to **the Yamaguchi Four Component Scattering Power Decomposition (4-CSPD) method**. After finding suitability of **4-CSPD method** over Himalayan glaciated terrain, it has been combined with complex Wishart distribution for supervised classification of ALOS-PALSAR image. By this way, an overall accuracy has been found to be 93.38%. Even this procedure shows very high accuracy but discrimination between vegetation and glacier snow/ice classes was not properly. To overcome this ambiguity, the probability difference between surface backscattering and volume backscattering has been introduced as further steps in classification procedure.

Keywords---Decomposition, PALSAR, **Himalayan**, glaciated terrain.

1. INTRODUCTION

Satellite remote sensing has great potential in the study of dynamically changing environments related to the high altitude cold regions mainly because of its repetitive capability and synoptic coverage. The land-covered features have unique reflectance characteristics in different spectral bands of optical sensors, which may provide information on physical properties as well as the areal extent of glaciated terrain features under cloud free conditions. However, they have some difficulty in rugged high mountainous area: 1) optical images are often affected by clouds in mountainous glacier areas. The Himalayan region is strongly affected by monsoons, cloud cover is quite common, especially during the summer months. The glaciated terrain classification is even hindered in Himalayan region due to a lack of cloud-free optical images; 2) the mountain shadow makes it difficult to discriminate between glacier areas and non-glacier areas and 3) an ambiguity between snow and ice exists because both have similar optical properties in glacial areas (Racoviteanu et. al., 2009). Due to the strong spatial and time dependent dynamics of glaciated terrain, regular and frequent mapping is necessary to monitor glaciated terrain, and requires sensors that are time and weather independent. Synthetic Aperture Radar (SAR) remote sensing with its all-weather capability, cloud penetration, and independence of sun illumination can add considerable robustness to classify the glaciated terrain (Rott, 1994; Singh and Venkataraman, 2009). In case of monostatic fully polarimetric SAR data, **point targets are** characterized by five parameters (three amplitude and two relative phases). Therefore SAR full polarimetry techniques can lead to a significant improvement in the quality of classification and segmentation results in comparison to conventional single-channel SAR. Fully polarimetric SAR also allows a discrimination of different types of scattering mechanisms. This becomes possible because the

received power **depends** strongly on the actual backscattering process. Received backscattering power can be divided into a sum of various backscattering contributions by using polarimetric target decomposition **methods** (Cloude and Pottier, 1996). Thus polarimetric decomposition **method** can be utilized for extracting the corresponding target type in fully polarimetric ALSO-PALSAR **images** over glaciated terrain.

In literatures (Cloude and Pottier, 1996; Yamaguchi, 2007; Lee and Pottier, 2009; Cloude, 2009) polarimetric target decomposition methods are categorized into two types: The first type is coherent decomposition **methods** which are directly performed on the scattering matrix. The second type is incoherent decomposition **methods** based on the second order statistics of polarimetric information, e.g. on the coherency matrix. **The incoherent decomposition** methods (Freeman and Durden, 1998; Yamaguchi et. al., 2006; Yajima et. al., 2008) decompose the coherency matrix as the incoherent sum of scattering power of a distributed target. Since most of the targets are distributed in natural earth surface, this type of target can be only characterized statistically. Singh (2010) proved that incoherent decomposition provides sufficient information for classification in glaciated terrain features such as debris covered ice, snow, barren rock, etc, using fully polarimetric data.

In this work, **the Yamaguchi four-component scattering power decomposition (4-CSPD) method (Yamaguchi et. al., 2006; Yajima et. al., 2008) is applied to identify glaciated terrain features in part of Indian Himalaya. The 4-CSPD method decomposes polarimetric radar power into surface, double bounce, volume, and helix power scattering. This method is an extension of the Freeman and Durden three-component scattering power decomposition (3-CSPD) method (Freeman and Durden, 1998) to general scattering case with non-reflection symmetry condition. However, the 4-CSPD methods has the following advantages: 1)**

Straightforward implementation; 2) Scattering power calculations are easy; 3) The decomposed powers correspond to physical scattering mechanisms, i.e., surface scattering, double bounce scattering , volume scattering , helix (circular polarization) scattering; 4) Output color-coded images are directly recognizable and easy to understand. Moreover this paper presents the **4-CSPD method** (Yamaguchi et. al., 2006; Yajima et. al., 2008) suitability as compared to the **3-CSPD method** (Freeman and Durden, 1998) **for glaciated terrain features identification.** A new methodology has been discussed by combining the complex Wishart distribution (Wishart, 1928) and **4-CSPD method** for glaciated terrain classification.

2. STUDY AREA

The location map is shown in Fig.1. The Alaknanda river catchment, Uttarakhand, India has many glaciers. Satopanth and Bhagirath Kharak glaciers are the major glaciers among them in this catchment. **The Satopanth and Bhagirath Kharak glaciers are approximately 13 and 18.5 km long with an average width of 750–850 m, covering an area of 21.17 and 31.17 km^2 respectively. The upper Alaknanda river catchment covers an area of 1544.08 km^2, out of which 70.70 and 107.22 km^2 are covered by the Satopanth and Bhagirath Kharak sub-watersheds, respectively (Nainwal et al., 2008).**

The elevation ranges between 2000 m.a.s.l (meters above sea level) and 7000 m.a.s.l. The Alaknanda river, which is the main tributary of Ganga river, originates at the snout of the Satopanth glacier. The area falls between latitude 30^0 40’ N and 30^0 50’ N and longitude between 79^0 15’ E and 79^0 28’ E. **Satopanth and Bhagirath Kharak glaciers are shown in Fig. 2(a) to (d). This glaciated region includes snow, debris covered glacier, and barren rocks targets.**

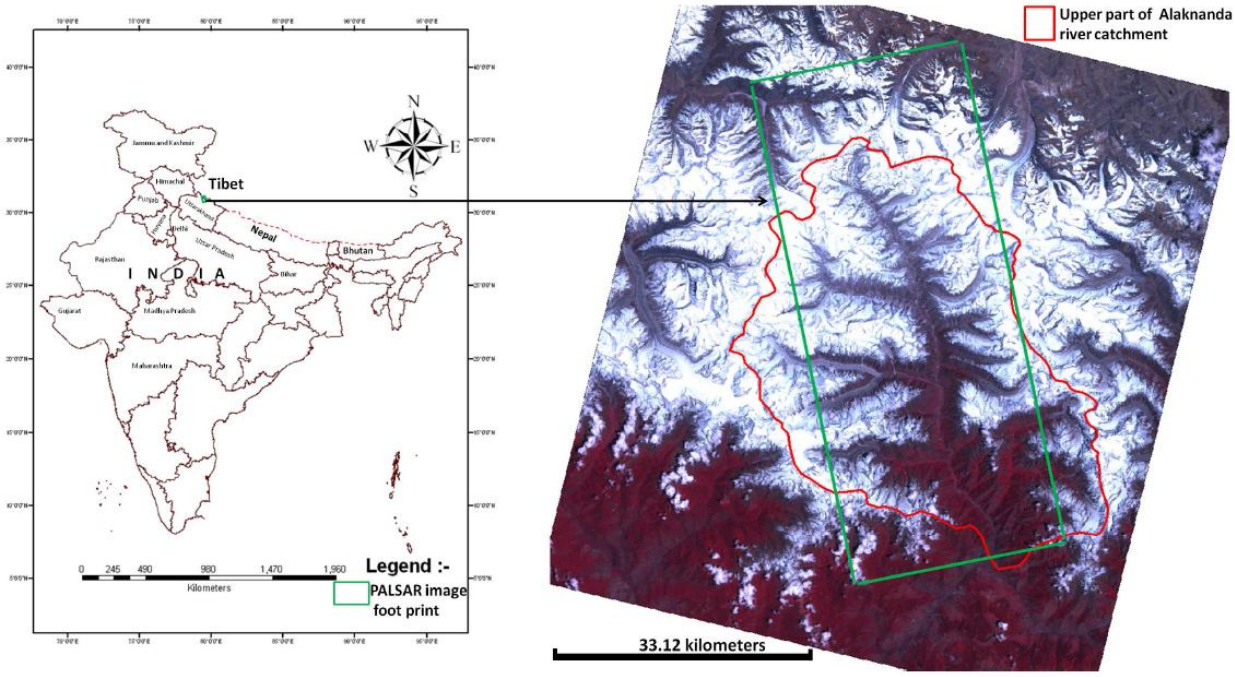

Fig.1. Location map of study area.

3. DATA USED

In this study, we acquired the Phased Array type L-band Synthetic Aperture Radar (PALSAR) fully polarimetric, single look complex, level 1.1 data of May 12, 2007 with 21.5^0 incident angle and nominal pixel spacing (azimuth x range) 3.54 (m) x 9.36 (m). PALSAR, on-board the Advanced Land Observing Satellite (ALOS), was launched on 24 January 2006 by the Japan Aerospace Exploration Agency (JAXA). It operates in the L-band frequency of 1.27 GHz (23.6 cm wavelength). It is well known that L-band microwave signals penetrate through dry snowpack with negligible volume backscatter from snow. However, if snowpack is wet, the situation becomes different. If the moisture exceeds 1% in highly accumulated snowpack, L-band frequency suffers from attenuation in the snowpack while reflection or backscatter from the snowpack comes out (Abe et. al. 1990). In general, snow cover area becomes wet in May (early summer) over Himalayan snow bound area with significant melting.

The magnitude of backscatter depends on the snow density and water content, and the depth of snowpack. Since the snowpack on May 06, 2007 is rather wet due to the beginning of snow melting, the snowpack contains water and is not so transparent for L-band frequency. Snowpack is also heterogeneous with snow grain particle compressed during winter season and contains rather high density due to snow accumulation and melting cycle. **The co-polarization backscatters (HH and VV) increases with snow volume, while the cross-polarization backscatter (HV) remains small as compared to co-polarization. Since the HV components contribute only to volume scattering, the main polarimetric response from snowpack becomes surface scattering in the L-band (Abe et. al. 1990).** Fig. 2(b) shows **the** Pauli color composite image (May 12, 2007) which gives the clear information about single scattering (snow cover area over glacier and non glacier), double bounce (dihedral features) and volume scattering (debris covered glacier) in the study area.

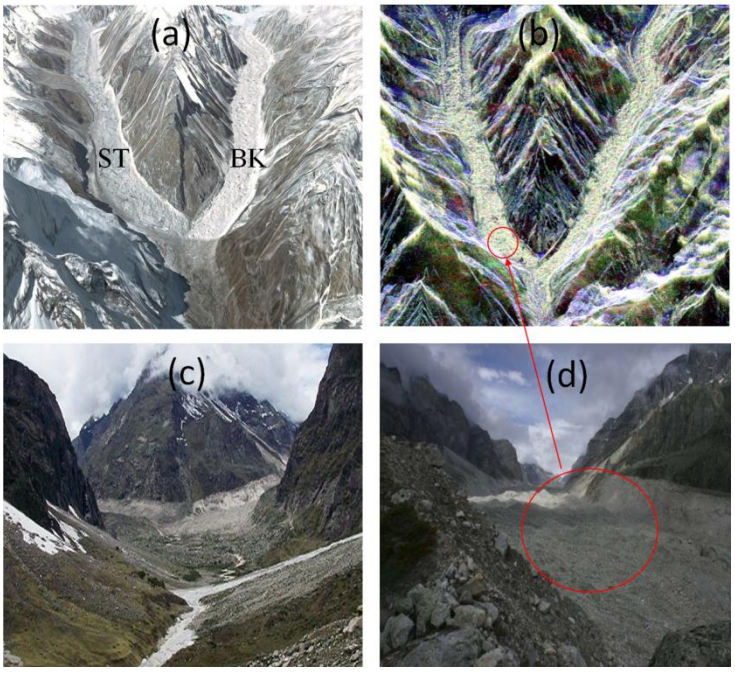

Fig.2. (a) 3-D View of Google Earth image (b) Pauli RGB of PALSAR of May 12, 2007(c) Photo of Satopanth (ST) and Bhagirath Kharak (BK) entrance (d) Photo view of Satopanth glacier

4. METHOD AND TECHNIQUE

4.1. Decomposition Method

Once scattering matrix **S** is acquired with fully polarimetric radar, we can define **the** scattering vector **k** as

$$k = \frac{1}{\sqrt{2}} \begin{bmatrix} S_{HH} + S_{VV} \\ S_{HH} - S_{VV} \\ 2S_{HV} \end{bmatrix} \quad (1)$$

where S_{HH}, S_{VV}, S_{HV} are elements of scattering matrix **S** assuming the reciprocal condition of $S_{HV} = S_{VH}$.

The coherency matrix is given as

$$[T] = \langle k.k^{*T} \rangle = \begin{bmatrix} T_{11} & T_{12} & T_{13} \\ T_{21} & T_{22} & T_{23} \\ T_{31} & T_{32} & T_{33} \end{bmatrix} \quad (2)$$

where $*^T$ denotes complex conjugation and transposition, and ‹•› denotes ensemble average in an imaging window.

The four-component scattering power decomposition method divides the measured coherency matrix into 4 sub-matrices representing physical scattering mechanisms (Yamaguchi et. al., 2006; Yajima et. al., 2008)

$$[T] = f_s[T_s] + f_d[T_d] + f_v[T_v] + f_c[T_c] \quad (3)$$

where f_s, f_d, f_v and f_c are coefficients to be determined. [Ts], $[T_d]$, $[T_v]$ and $[T_c]$ are expansion coherency matrices corresponding to surface, double bounce (DB), volume, and helix scattering, respectively.

The single-bounce scattering model is represented by surface scattering phenomena from slightly rough surface in which the cross-polarized component is negligible. The expansion coherency matrix for surface scattering is

$$[T_s]=\begin{bmatrix}1 & \beta^* & 0\\ \beta & |\beta|^2 & 0\\ 0 & 0 & 0\end{bmatrix},\quad |\beta|=\left|\frac{S_{HH}-S_{VV}}{S_{HH}+S_{VV}}\right|<1 \qquad \textbf{(4)}$$

The double-bounce scattering model is based on the hypothesis of double reflections from right angle structures. Double-bounce structure includes road surface—building wall, ground-trees, and man-made targets etc.. The expansion coherency matrix for double bounce scattering is

$$[T_d]=\begin{bmatrix}|\alpha|^2 & \alpha & 0\\ \alpha^* & 1 & 0\\ 0 & 0 & 0\end{bmatrix},\quad |\alpha|=\left|\frac{S_{HH}+S_{VV}}{S_{HH}-S_{VV}}\right|<1 \qquad \textbf{(5)}$$

Volume scattering can be observed if SAR beam penetrates into a medium. Scattering by trees or branches, subsurface or snow/ice layers etc. are examples of volume scattering. For the volume scattering model, we choose one of the following matrices according to the magnitude balance of $|S_{HH}|^2$ and $|S_{VV}|^2$ (Yamaguchi *et al.*, 2006)

When 10log ($\langle|S_{VV}|^2\rangle / \langle|S_{HH}|^2\rangle$) ≥2 dB

$$[T_V]=\frac{1}{30}\begin{bmatrix}15 & -5 & 0\\ -5 & 7 & 0\\ 0 & 0 & 8\end{bmatrix} \qquad \textbf{(6)}$$

When |10log ($\langle|S_{VV}|^2\rangle / \langle|S_{HH}|^2\rangle$) | < 2 dB

$$[T_V]=\frac{1}{4}\begin{bmatrix}2 & 0 & 0\\ 0 & 1 & 0\\ 0 & 0 & 1\end{bmatrix} \qquad \textbf{(7)}$$

When 10log ($\langle|S_{VV}|^2\rangle / \langle|S_{HH}|^2\rangle$) ≤ -2 dB

$$[T_v] = \frac{1}{30}\begin{bmatrix} 15 & 5 & 0 \\ 5 & 7 & 0 \\ 0 & 0 & 8 \end{bmatrix} \quad \textbf{(8)}$$

Helix scattering power is equivalent to circular polarization power. This term appears in urban and mountainous area for L-band data. The helix scattering expansion matrix, which takes into account of non-reflection symmetry condition, is

$$[T_c] = \begin{bmatrix} 0 & 0 & 0 \\ 0 & 1 & \pm j \\ 0 & \mp j & 1 \end{bmatrix} \quad \textbf{(9)}$$

The corresponding scattering powers (the surface scattering power P_s, the double bounce scattering P_d, the volume scattering power P_v and the helix scattering power P_c) are directly obtained from the expansion coefficients when we applied decomposition. The decomposition takes account of an imbalance of the co-polarized channel power. For the case of $|10\log(\langle|S_{VV}|^2\rangle / \langle|S_{HH}|^2\rangle)| < 2$ dB, the decomposed power expression becomes as (Yamaguchi, 2007):

$$P_c = f_c = 2|\mathrm{Im}\{T_{23}\}| \quad \textbf{(10.1)}$$

$$P_v = f_v = 4T_{33} - 2P_c \quad \textbf{(10.2)}$$

$$P_s = f_s(1+|\beta|^2) \quad \textbf{(10.3)}$$

$$P_d = f_d(1+|\alpha|^2) \quad \textbf{(10.4)}$$

3.2. Complex Wishart Classifier

The complex Wishart distribution is expressed as (Wishart, 1928)

$$P\left(\langle T\rangle / T_m\right)=\frac{L^{Lp}\left|\langle T\rangle\right|^{L-P} e^{-L\mathrm{Tr}\left(\left[T_m\right]^{-1}\langle T\rangle\right)}}{\pi^{\frac{p(p-1)}{2}}\Gamma(L)...\Gamma(L-p+1)\left[T_m\right]} \quad \textbf{(11)}$$

Where L is **the** number of looks and p is **the** polarimetric dimension and $\mathbf{[T_m]}$ = E($\mathbf{k\ k^{T*}}$). Using the complex Wishart distribution of the coherency matrix <**T**>, an appropriate distance measure, d, can then be calculated according to Bayes maximum likelihood classification as (Lee and Pottier, 2009)

$$d_m\left(\langle T\rangle\right)=L\mathrm{Tr}\left(\left[T_m\right]^{-1}\langle T\rangle\right)+L\ln\left(\left[T_m\right]\right)-\ln\left(P\left(\left[T_m\right]\right)\right)+K \quad \textbf{(12)}$$

Thus leading to a minimum distance classification independent of the number of looks used to form the multi-looked coherency matrix <**T**> (Lee and Pottier, 2009):

$$\langle[T]\rangle \in [T_m] \quad \text{if} \quad d_m\left(\langle[T]\rangle\right)<d_j\left(\langle[T]\rangle\right) \quad \forall j\neq m \quad \textbf{(13)}$$

3.3. Decomposed Power Probability

The 4-CSPD method decomposes total backscattering power into surface scattering (P_s), double bounce backscattering (P_d), volume backscattering (P_v), and helix backscattering (P_c). Total backscattering power (TP) can defined as

$$TP=P_s+P_d+P_v+P_c \quad \textbf{(14)}$$

With the help of equation (7), we can define the probability of surface backscattering and volume backscattering decomposed components as

Probability of surface backscattering, $$P_{surface} = \frac{P_s}{TP} \quad \textbf{(15)}$$

Probability of volume backscattering $$P_{volume} = \frac{P_v}{TP} \quad \textbf{(16)}$$

Therefore from (8) and (9)

$$-1 \le \Delta P_{s-v} = P_{surface} - P_{volume} \le 1 \quad \textbf{(17)}$$

Eq. (17) helps us to determine the dominated scattering component from surface scattering and volume scattering in the 4-CSPD method's decomposed image. If ΔP_{s-v} is positive, we determine that surface scattering is the dominant contribution. On the other hand, if ΔP_{s-v} is negative, we determine that volume scattering is the dominant contribution. The threshold has not been started from zero because we want to take into account the noise variation in case that both the probabilities are close to zero.

3.4. Classification Procedure

Using **4-CSPD method** and Complex Wishart Distribution (CWD), a supervised classification methodology has been presented for fully polarimetric SAR images classification. The flow chart of developed methodology is shown in Fig, 3.

The sequence of this procedure is followed as:

1. First of all, a multi-looked (6 times in azimuth direction and 1 times in range direction) coherency matrix has been generated.

2. For reduction the speckle noise from the polarimetric SAR data, the polarimetric refined Lee filter (Lee et. al, 1999) with window size 7×7 has been applied on coherency matrix.
3. **4-CSPD** method has been applied on de-speckled coherency matrix and **4-CSPD method** false color composite (FCC) image has been generated. In **4-CSPD method** FCC image, red color is assigned to double bounce scattering, green color is assigned to volume scattering and blue color is assigned to surface scattering. Training samples has been allotted on the basis of visually comparing four component color composite image with AVNIR-2 snow cover image and field information.
4. CWD has been applied on despeckled coherency matrix and computed the averaged coherency matrices from the assigned classes. These computed mean matrices have been used as the class centers. All pixels are classified based on their Wishart distance measure and criteria **(Eq. (12) and eq. (13))** from class centers.
5. Finally based on conditional approach, the probability difference ($\Delta P_{s\text{-}v}$) has been used for resolving volume scattering ambiguity from vegetation and glacier snow/ice. The conditional approach is defined as

   EITHER glacier snow/ice class IF ($\Delta P_{s\text{-}v} \geq 0.05$ && vegetation class) OR classified classes

   OTHERWISE

   i.e. an additional class (glacier snow/ice class) has been added to supervised classified image, where is, the probability difference ($\Delta P_{s\text{-}v}$) image has ≥0.05 value but supervised classified image shows vegetation class. Otherwise supervised classified pixels remain same in final classified image.

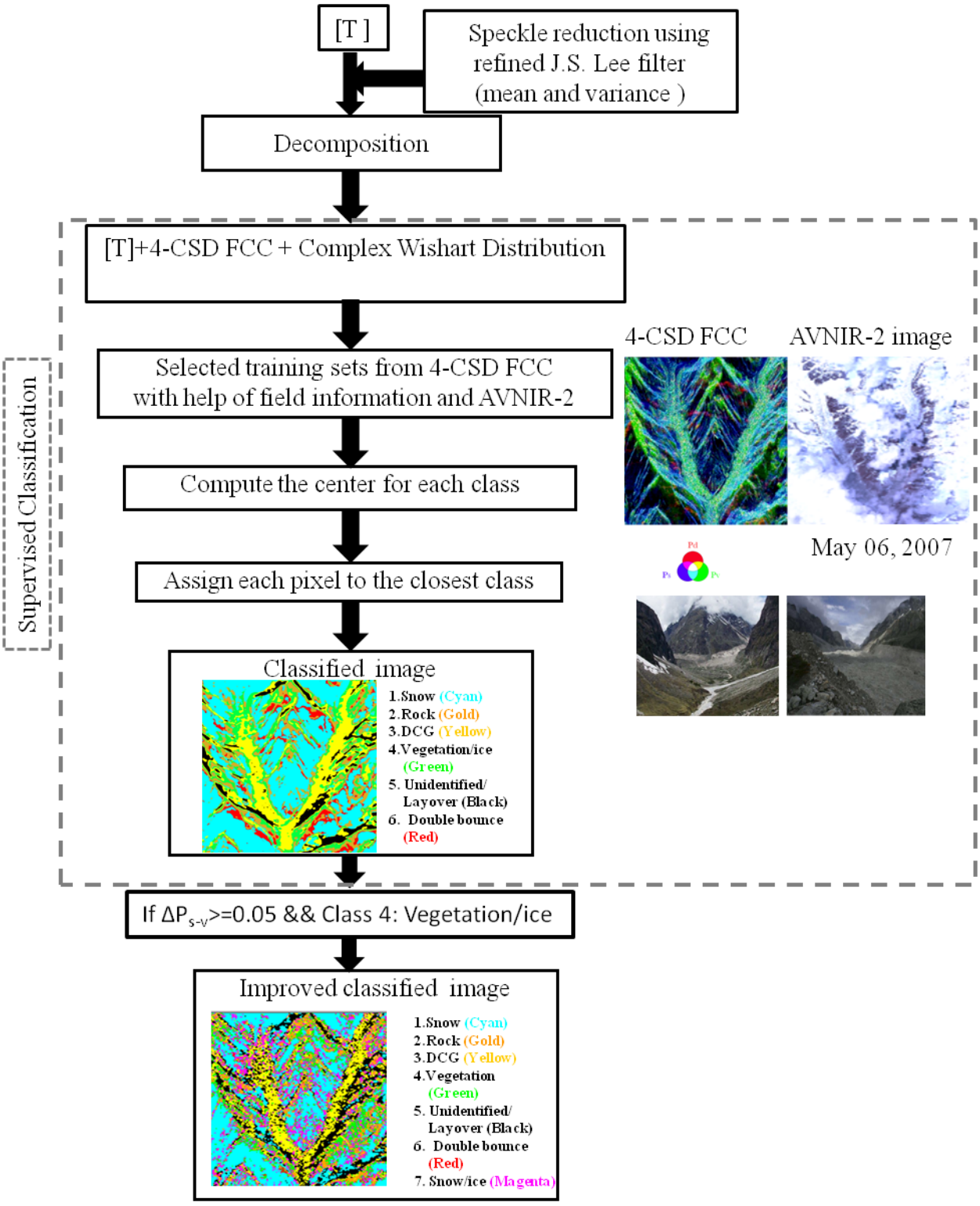

Fig. 3. Flow chart of PALSAR image classification

4. RESULTS AND DISCUSSION

The **3-CSPD and 4-CSPD methods** have been applied on L-band PALSAR data over the Satopanth and Bhagirath Kharak glaciated region. **3-CSPD and 4-CSPD methods** false color composite (FCC) images are shown in Fig.4. In **3-CSPD and 4-CSPD methods** FCC images of PALSAR data over Satopanth glacier region (Fig. 4), blue to deep blue colour represents surface scattering from snow cover over glacier area (accumulation zone) and permanent snow cover at mountains peaks. Red colour represents double bounce or dihedral scattering mechanism. Debris covered glaciers (ablation area) are shown in green colour. Glacier moraines dam lakes appear in deep blue color.

The comparison of visual interpretation has been done for both decomposed FCCs with the Pauli RGB (Fig. 2(b)) and AVNIR-2 (Fig.4) image. The differences are clearly seen between **3-CSPD and 4-CSPD methods** FCCs in Fig.5 (enlarged part of red color rectangular area in Fig. 4). Most of the differences can be visibly identified in double bounce and surface scattering component and these components are clearly exposed (Fig. 5(b)) in **4-CSPD method** FCC. Some of these differences are indicated by yellow circles number 1, 2 and 3 in Fig. 5(b) **(4-CSPD FCC)** correspond to yellow color circles no. 1, 2 and 3 in Fig. 5(a) (**3-CSPD FCC**) respectively. Furthermore, **4-CSPD method** gives very sharp information about dihedral features in the study area as compared to **3-CSPD method** and Pauli RGB images. Since, the 4^{th} component of four component scattering decomposition (**4-CSPD**) method represents the helical scattering phenomena, which occur due slope surface of target. **It has been seen in Fig.6 that the helix (Pc) scattering component shows high value (> -10 dB) at steep slope and low values (<-20 dB) are found over snow covered area. Himalayan topography has gentle to steep slope, which behave like oriented target from the direction of radar and oriented target does not hold**

reflection symmetry condition where the 3-CSPD method works, which causes the over estimation volume scattering in 3-CSPD method. But in 4-CSPD method, volume scattering is reduced by the 4th component where volume scattering is more than helix scattering component. **The main reason for the reduction of the volume component for the 4-CSPD method is due to the reflection symmetric space where the 4-CSPD method works. In other words, it correct for rotation along the line of sight (LOS) while it decomposes.** Therefore, a **4-CSPD method** is suitable for fully polarimetric PALSAR data decomposition over Himalayan glaciated terrain as compared to **3-CSPD method.**

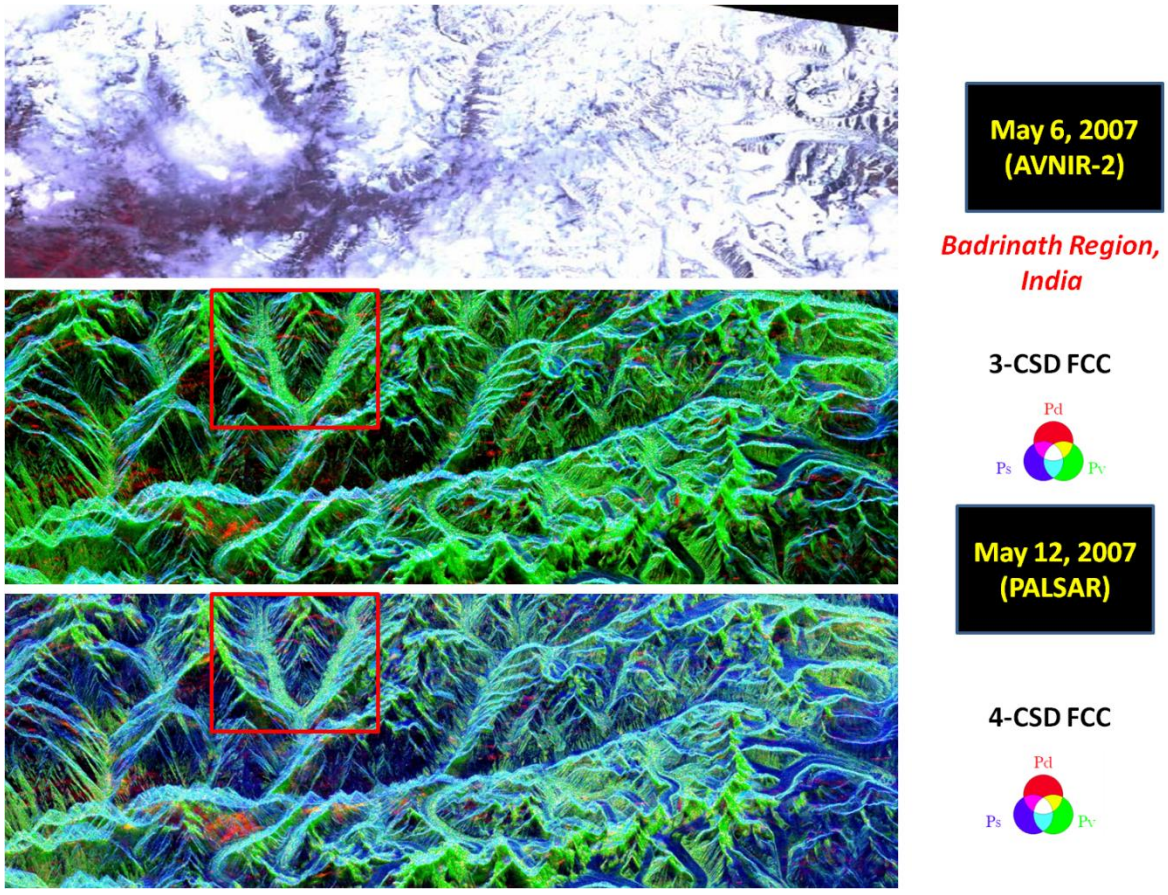

Fig. 4. ALOS-AVNIR-2 image of May 6, 2007 (upper), and 3-CSD model FCC of May 12, 2007 PALSAR data (middle) and 4-CSD model FCC of May 12, 2007 PALSAR data (bottom) (Red color rectangular on 4-CSD model FCCs enlarged view are shown in Fig. 5)

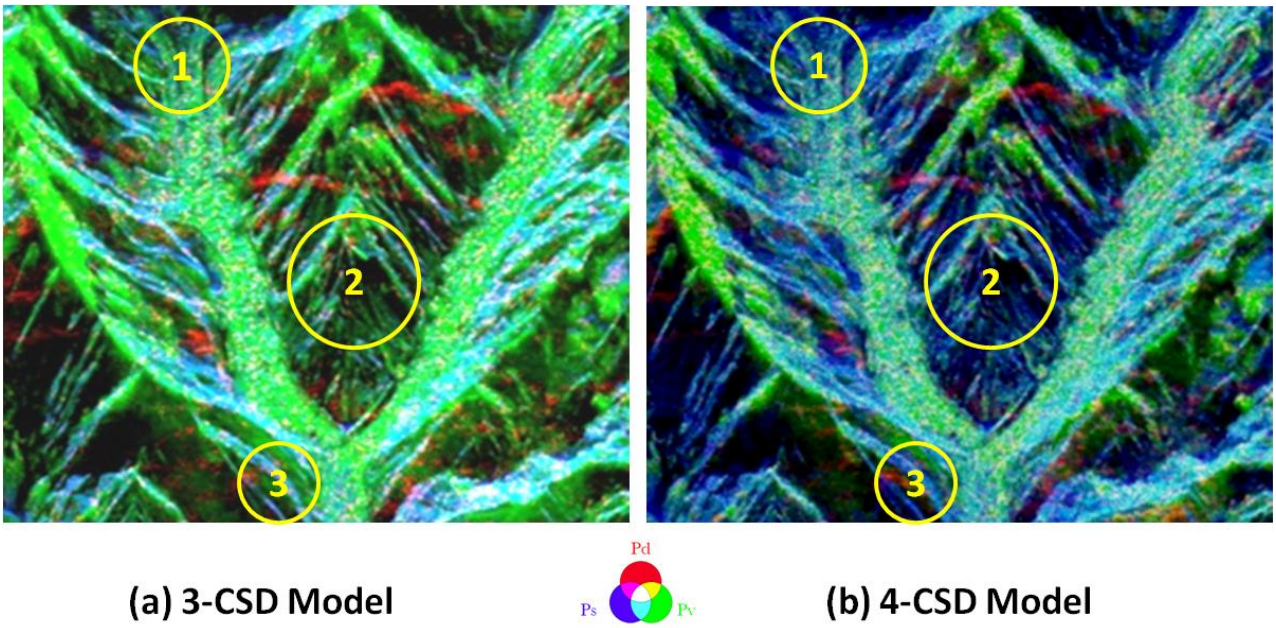

Fig. 5. (a) 3-CSD Model FCC of May 12, 2007 PALSAR data (b) 4-CSD Model FCC of May 12, 2007 PALSAR data

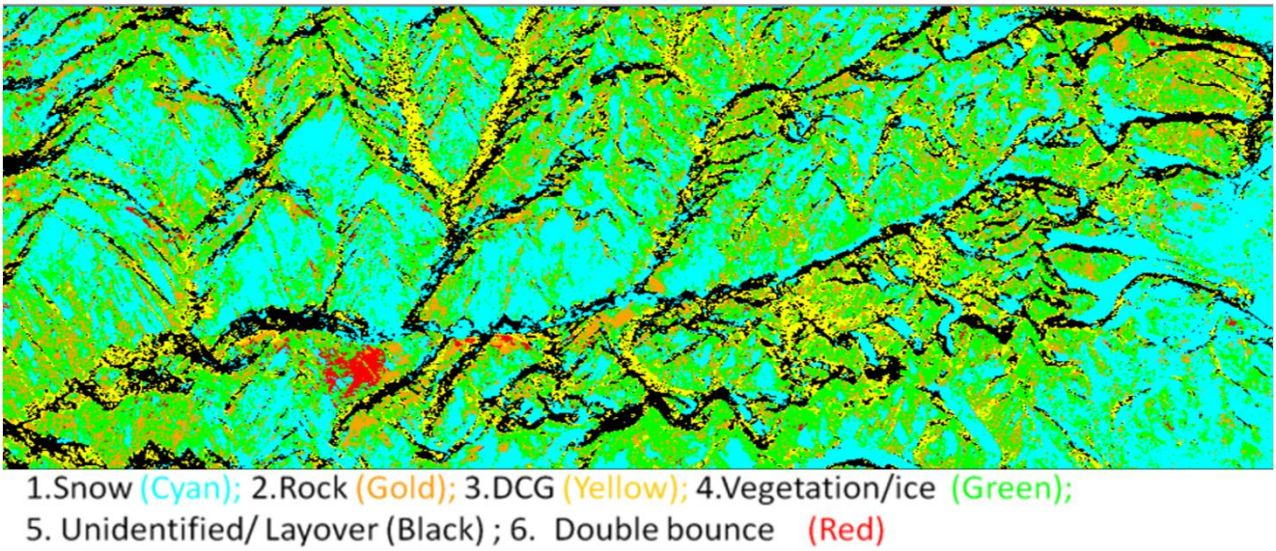

Fig. 6. PALSAR classified image of May 12, 2007

Moreover, using **4-CSPD method** decomposed image and complex Wishart distribution, ALOS PALSAR data was classified into six major classes (e.g. snow, non snow and unidentified/layover,

Fig. 7). Classification technique was applied on coherency matrix and training samples were taken from the four component color composite image with help of visual interpretation of **4-CSPD method** FCC and AVNIR-2 image (which are shown in Fig.4).

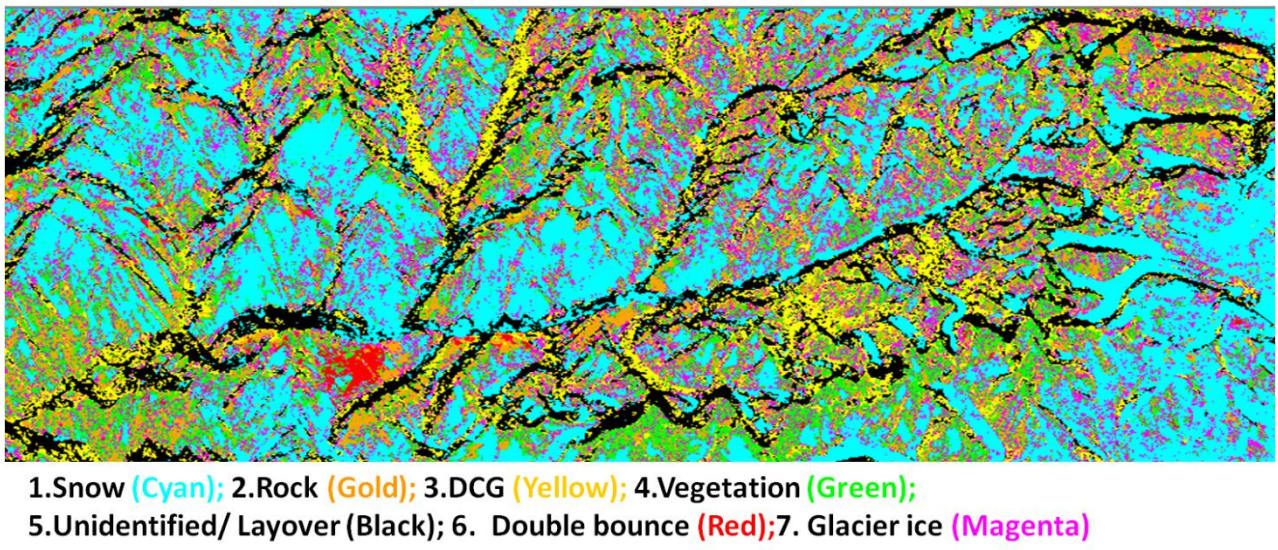

Fig. 7. Vegetation and ice separating in PALSAR classified image of May 12, 2007 by using probability difference between surface scattering and volume scattering probabilities

The most common tool used for assessing the classification accuracy is the confusion (or error) matrix (Table 1). The columns in a confusion matrix (Table 1) represent test data that have been collected via field observation and interpretation of **4-CSPD method** FCC and ALOS AVNIR-2 image, while rows represent the labels assigned by the classifier. The main diagonal entries of the Table 1 represent the number of pixels that are correctly classified. By this way, overall classification accuracy has been found to be 93.38%. While both user's accuracy and producer's accuracy of vegetation class are more than 80%, but vegetation class from glacier snow/ice could not discriminated properly by using alone complex Wishart classifier with defined training samples. For further improvement of classified image **(Fig.7)**, a probability difference

image (ΔP_{s-v}) has been used for separating these classes. The probability difference image shows the low value over vegetation area and high value over glacier snow/ice area. By using conditional approach, it is possible to resolve the ambiguity between vegetation class **(Fig.6)** and glacier snow/ice **(Fig. 7)**.

Table 1. A confusion matrix composed of six glaciated terrain classes.

	Snow	Rock	DCG	Double Bounce (DB) /Settlement	Vegetation/ice	Layover	Row Sum
Snow	**19885**	67	73	0	87	65	20177
Rock	106	**1594**	0	29	282	0	2011
DCG	0	0	**3629**	0	94	469	4192
DB/Settlement	0	72	0	**742**	11	0	825
Vegetation/ice	0	477	224	0	**3072**	13	3786
Layover	0	0	32	0	0	**735**	767
Column Sum	19991	2210	3958	771	3546	1282	**31758**
Producer's Accuracy (%)	**99.46**	**72.12**	**91.68**	**96.24**	**86.63**	**57.33**	
User's Accuracy (%)	**98.55**	**79.25**	**86.58**	**89.96**	**89.96**	**95.86**	**Overall accuracy** = 93.38%

5. SUMMARY AND CONCLUSION

In this work, full polarimetric PALSAR data has been analyzed of high altitude glaciated terrain in Himalayan region based on **3-CSPD and 4-CSPD** methods and information of various terrain features has been extracted. It has been found that the **4-CSPD method** discriminates better terrain features like snow cover, dihedral (double bounce) and glacier features as compared to **3-CSPD method.**

The supervised classification procedure shows over all accuracy 93.38% but the ambiguity of separating the vegetation from glacier snow/ice has been also found in classified image. Therefore, the probability difference (ΔP_{s-v}) has been combined with supervised classification procedure to resolve the ambiguity between vegetation and glacier snow/ice. In future work, this methodology will be assessed with more time series data to check the resolving capability of the ambiguity between vegetation and glacier snow/ice.

ACKNOWLEDGEMENT

The authors would like to thank JAXA for providing ALOS-PALSAR data free under RA project (JAXA-555).

REFERENCES

Abe T., Yamaguchi Y. and Sengoku M., 1990. Experimental study of microwave transmission in snowpack, *IEEE Transactions on Geoscience and Remote Sensing*, 28 (5), 915-921.

Cloude, S.R., and Pottier, E., 1996. A review of target decomposition theorems in radar polarimetry. *IEEE Transactions on Geoscience and Remote Sensing*, 34, 498–518.

Cloude ,S. R.,2009. *Polarisation: Applications in Remote Sensing.* Oxford University Press, 2009

Freeman, A., and Durden, S. L., 1998. A three-component scattering model for polarimetric SAR data. *IEEE Transaction on Geoscience and Remote Sensing*, 36(3), 936–973.

Lee, J. S., Grues, M. R., and de Grandi, G., 1999. Polarimetric SAR speckle filtering and its implication for classification. *IEEE Transactions on Geoscience and Remote Sensing*, 37, 2363-2373.

Lee,J.S., and Pottier, E.,2009.*Polarimetric radar imaging: from basics to application,* CRC Press, Taylor & Francis Group, Boca Raton.

Nainwal H. C., Negi B. D. S., Chaudhary M., Sajwan K. S. and Gaurav Amit, 2008. Temporal changes in rate of recession: Evidences from Satopanth and Bhagirath Kharak glaciers, Uttarakhand, using Total Station Survey, *Current Science*, 94 (5), 653-660.

Racoviteanu, A. E., Paul, F., Raup, B., Khalsa, S.J.S., Armstrong, R., 2009. Challenges and recommendations in mapping of glacier parameters from space: results of the 2008 Global Land Ice Measurements from Space (GLIMS) workshop, Boulder, Colorado, USA. Annals of Glaciology, 50(53), 53-69.

Rott, H., 1994. Thematic studies in alpine areas by means of polarimetric SAR and optical imagery. *Advances in Space Research*, 14(3), 217-226.

Singh, G. and Venkataraman, G., 2009. LOS PALSAR data Analysis of snow cover area in Himalayan region using four component scattering decomposition model. In: *Proceedings* o*f IEEE Micowave08*, Jaipur, India, 772-774.

Singh, G., 2010. *SAR polarimetry techniques for snow parameters estimation*. Ph.D. Thesis, Indian Institute of Technology Bombay, India.

Wishart, J., 1928. The generalised product moment distribution in samples from a normal multivariate population. *Biometrika*, 20A (1-2), 32–52.

Yajima, Y., Yamaguchi, Y., Sato, R., Yamada, H. and Boerner, W.M., 2008. POLSAR image analysis of wetlands using a modified four-component scattering power decomposition. *IEEE Transaction on Geoscience and Remote Sensing*, 46(6), 1667-1673.

Yamaguchi, Y., Yajima, Y. and Yamada, H. , 2006.A four-component decomposition of POLSAR images based on the coherency matrix. *IEEE Geoscience and Remote Sensing Letter*, 3(3), 292–296.

Yamaguchi, Y., 2007. *Radar polarimetry from basics to applications: radar remote sensing using polarimetric information (in Japanese).* IEICE, Japan (ISBN978-4-88552-227-7).